Wake interaction in offshore wind farms with mesoscale derived inflow condition and sea waves

Wake interaction in offshore wind farms with mesoscale derived inflow condition and sea waves

A. Castorrini[1], L. Tieghi[2], V.F. Barnabei[2], S. Gentile[3], A. Bonfiglioli[1], A. Corsini[2], F. Rispoli[2].
1 School of Engineering, University of Basilicata, Potenza, Italy
2 Department of Mechanical and Aeronautical Engineering, University of Rome La Sapienza, Roma, Italy
3 CNR Italian National Research Council – IMAA, Tito Scalo (PZ), Italy

E-mail: alessio.castorrini@unibas.it

Abstract. Numerical simulation is an indispensable tool for the design and optimization of wind farms layout and control strategies for energy loss reduction. Achieving consistent simulation results is strongly related to the definition of reliable weather and sea conditions, as well as the use of accurate computational fluid dynamics (CFD) models for the simulation of the wind turbines and wakes. Thus, we present a case study aiming to evaluate the wake-rotor interaction between offshore multi-MW wind turbines modelled using the Actuator Line Model (ALM) and realistic wind inflow conditions. In particular, the interaction between two DTU10 wind turbines is studied for two orientations of the upstream turbine rotor, simulating the use of a yaw-based wake control strategy. Realistic wind inflow conditions are obtained using a multi-scale approach, where the wind field is firstly computed using mesoscale numerical weather prediction (NWP). Then, the mesoscale vertical wind profile is used to define the wind velocity and turbulence boundary conditions for the high-fidelity CFD simulations. Sea waves motion is also imposed using a dynamic mesh approach to investigate the interaction between sea waves, surface boundary layer, and wind turbine wakes and loads.

1. Introduction

Off-shore wind power represents the most promising branch of the wind technology, because of the availability of high-speed wind resource and large areas available to build the power plants. Wind turbines clustering, however, leads to the interaction of the wake generated by upstream turbines over the downstream ones, resulting in an unbalanced power production and uncontrolled structural loads. For this reason, it is crucial to design and optimize the wind farm layout to maximize the power production and control the wake losses. In addition, control strategies have been proposed and developed in recent years to reduce the cumulative effect of wake losses. These control strategies are mostly based on the deflection of front turbines wake through a rotor-wind misalignment (non-zero yaw angle). Examples are the work of [1], in which an optimal yaw control law has been evaluated on a six turbines wind farm layout, showing that the maximum cumulative power output could be reached for non-zero yaw angles assigned to the upstream rotors. Another example is [2], where the authors used wind tunnel tests to optimize the total power output and found an optimal yaw angle ranging between 16° and 20°.

Most of the studies about wind farm wakes use the actuator line model (ALM) and a standard approach to simulate the wind field based on the Reynolds Averaged Navier-Stokes (RANS) or Large Eddy Simulation (LES) [1]. The wind conditions implemented at the CFD boundaries usually employ reference wind profiles, either considering neutral stratification, or including corrections for non-neutral planetary boundary layer (PBL) based on the Monin-Obukhov Similarity Theory (MOST) [3]. However, wind turbine prototypes featuring 15 MW of rated power have rotor diameters up to 240 meters and tower heights in excess of 150 meters [4][5]. Therefore, a modern offshore wind turbine covers a large portion of the PBL, facing a wind flow characterised not only by different stability conditions, but also including large-scale convection, wind veer and non-monotonic variations of the velocity direction and magnitude with the elevation.

Mesoscale simulations can describe most of the abovementioned features of the real PBL, but typically feature low spatial resolution because of the large area (hundreds of kilometres) covered by the computational domain used in the meso-scale simulation. Multi-scale approaches based on the NWP/CFD coupling, such as the one used here, have demonstrated the capability to increase the spatial resolution on a specific target area, thus enabling the wind industry and academia to use realistic wind inflow in the study of wind farm aerodynamics [7].

Interface and coupling of mesoscale with local scale simulation of the wind has been extensively treated in the literature on pollutant transport [8], evaluation of wind and wind loads in urban areas [8], and wind energy [10][11][12][13]. A common approach consists in using the mesoscale simulation to generate boundary conditions for a local scale turbulent simulation on the wind farm area based on the Reynolds-Averaged Navier Stokes (RANS). In this approach, the RANS model is made consistent with the profile supplied by the mesoscale simulation by including appropriate modifications in the momentum and turbulence closure equations, and in the wall and inflow modelling. The framework that will be adopted in this study is the one developed in [7]: it relies on the RANS model adaptation proposed by Richards et al. [14], Temel et al. [15] and Sogachev et al.[16].

Although most of the studies about wind turbines (WTs) rely on a RANS numerical approach, the limitations of such methods in presence of unsteady phenomena are very well acknowledged [17]. Therefore, in this paper, the simulations that account for the presence of the WTs make use of an hybrid LES-RANS approach called Delayed Detached Eddy Simulation (DDES) [18]. The DDES is a variant of the standard DES model, with a different computation of the length scale. The DDES model achieves an LES level of accuracy in the detached flow and far field regions wherever the grid is sufficiently fine, whereas it reverts to RANS modelling in the boundary layer, but also in those far-field regions where the grid is coarse. The effectiveness of DDES in reproducing complex terrains features was already reported by Schulz et al. in [19], clearly highlighting the variation in power spectrum of the turbine with respect to a flat terrain. In [20] Sørensen et al. observed that standard RANS approaches overpredicted the mechanical power around wings and airfoils at higher wind speeds and that the transport of momentum far downstream are not correctly reproduced. Rahimi et al. [21] compared RANS and DDES modelling and found that the latter provides better resolution of the turbulent kinetic energy (TKE) and a more realistic vortex shedding.

In this paper the interaction between the WTs and the wind field is modelled using the ALM. ALM, first introduced by Sørensen in [22], amounts to add a source term in the Navier-Stokes equations that is based on the geometrical and aerodynamic characteristics of the WT. ALM has been successfully applied to a wide range of conditions, such as uniform or turbulent inflows [23][24]. Recently, ALM-based LES simulations were carried out to simulate the wind flow in wind farms [25]. In [26], a comparison between experimental measurements and both Actuator Disk Model and ALM is performed, highlighting a good agreement, with the ALM correctly reproducing complex flow features such as tip vortices. However, as pointed out in [27], there is still need to investigate the interactions between turbine wakes, especially in presence of real turbulent and unsteady aerodynamic flows.

In this study, we present an analysis of wake control and wake-rotor interaction using the ALM and an advanced CFD framework that allows to test the system taking into account a realistic wind inflow. We study a simple wind farm layout consisting of two 10MW turbines immersed in a wind field

obtained using a multi-scale simulation. The multi-scale approach combines mesoscale wind predictions obtained from an NWP code with local-scale turbulent flow simulations obtained from a CFD code. More precisely, the wind profile is obtained by downscaling the mesoscale wind prediction at a selected offshore site over a time-frame characterized by a non-uniform wind velocity profile. The WTs are aligned with the average wind direction and the upstream rotor is simulated both in wind-aligned and yawed conditions. For each of these two setups, we investigate the effects of the interaction between the wakes and the wind field, the wakes and the second rotor, and the effect of the yaw misalignment as a possible wake-loss-mitigation system. A preliminary unsteady RANS (URANS) simulation based on the k-ω SST model is used to downscale the mesoscale wind prediction, thus providing the local-scale wind profile at the site. Then, two DDES including the WTs as two ALM rotors, are performed to obtain the results. The presence of the sea waves is also accounted for in this study using a dynamic mesh approach, whereby the wave motion is prescribed using a dynamic displacement of the sea surface patch in the local-scale simulation.

2. Methodology

The methodology used in this paper consists in generating first a reliable wind inflow condition for the local-scale CFD simulations. This is done by performing a mesoscale simulation of the atmosphere in the region surrounding the target location selected for the test, which will be more precisely defined in Section 3. The result of the mesoscale simulation is used to generate boundary conditions for the local-scale simulation and then downscaled over the target area by performing a URANS simulation over a 10-minute time interval. Finally, a local-scale DDES simulation is performed which accounts for the presence of the WTs by means of the ALM.

The mesoscale simulation has been performed at the Institute of Methodologies for Environmental Analysis of the National Research Council (IMAA-CNR) using the WRF ARW system version 4.3 [28]. The WRF-ARW is released by the National Center for Atmospheric Research (NCAR, http://www.wrf-model.org), and it solves the Eulerian compressible non-hydrostatic equations, using a mass vertical coordinate varying with the height on a staggered Arakawa-C grid. The local resolution can be increased with one- or two-ways horizontal nesting. Several multiphysics parameterizations are available including cumulus convection, microphysics, radiation, planetary boundary layer and land-surface modelling [28][29]. In this work, the Mellor–Yamada Nakanishi and Niino Level 2.5 (MYNN2.5) [30] have been selected as PBL scheme. This scheme includes a closure equation for the TKE allowing the mesoscale simulation to provide boundary conditions also for the turbulent kinetic equation in the local-scale simulation.

The wind downscaling procedure follows the methodology presented in [7]. The target location is first identified on the map and made to coincide with the centre of the wind farm. This location is also taken as the centre of the CFD domain, whose lateral width is defined using the four neighbouring adjacent cells of the mesoscale grid as shown in Figure 1.

To generate the boundary conditions, the wind velocity components and turbulent kinetic energy at all vertical levels are exported from WRF-ARW in the form of time series within the 5x5 mesoscale grid-points surrounding the target location, see Figure 1. The data is interpolated at each local-scale time step over the boundaries of the local-scale domain using cubic interpolation. Linear interpolation is employed to project the time-dependent mesoscale data to the finer time scale used for the URANS and DDES simulations. We use a log-law to fit the vertical profile of the wind in the first 10 meters above the water surface, where mesoscale data are not available.

The boundary conditions and location of the top surface are selected in order to ensure that the local-scale solution close to the upper boundary of the CFD domain almost overlaps with the mesoscale prediction.

The turbulence closure model adopted in the local-scale simulations relies on the two equations k-ω SST model with model constants defined as prescribed in [16] and [15]. Additional source and sink

terms are added to the turbulence and momentum equations to account for Earth rotation, ambient turbulence, and geostrophic wind drag.

At the sea surface we account for the presence of small-scale roughness and resolved sea waves. In most RANS simulations of the PBL, the surface roughness and the flow field close to the sea (or terrain) are modelled using wall functions. In this study, we apply the model presented in [31], which is a variation of the standard wall functions corrected for PBL simulations. The roughness length used for the water surface is estimated using Charnock's relation [32] and set equal to $z_0 = 0.5$ mm.

The waves are also modelled in the simulation by prescribing the motion of the grid points at the sea surface using the following vertical displacement law (based on [33]):

$$H(t,x,y) = H_s \cos(k\, x \cos\theta + k\, y \sin\theta - 2\,\pi\, f\, t + \phi)$$

Here, H is the elevation of the water surface above the mean sea level (z = 0 m), f is the wave frequency, λ the wavelength, H_s the maximum amplitude, $k=2\pi\lambda$ is the wave number, θ is the angle between the x-axis (i.e. East direction of Figure 1) and the direction of wave propagation (we assume that the waves propagate in the same direction of the mean wind), ϕ is the phase angle, and x, y, and t are the sea surface and time coordinates. The displacement at the boundary is propagated using a dynamic morphing of the mesh based on [34][35]. In our case, the displacement H of the sea surface is prescribed as a time dependent boundary condition to a Laplacian solver, which computes the displacement of the internal grid nodes.

The local scale simulations have been performed using OpenFOAMv2012 [36], an opensource library largely adopted for CFD applications.

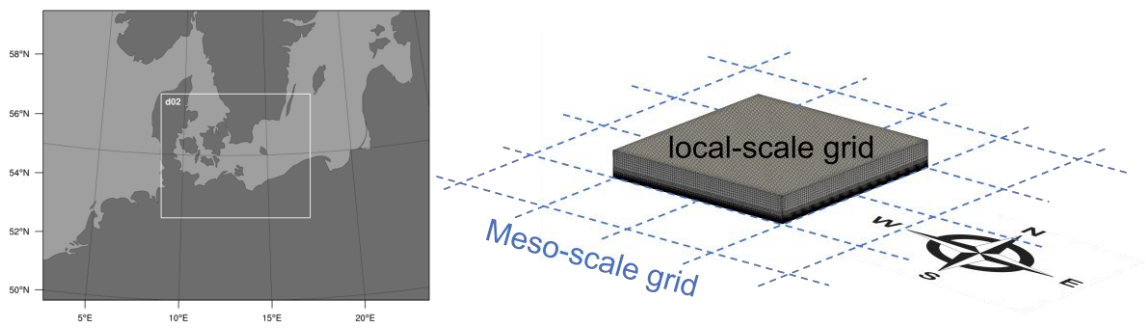

Figure 1 - Mesoscale and local-scale domains.

As already mentioned earlier, the two WTs are modeled using an ALM approach, which amounts to add source terms in the linear momentum equations that depend on both the geometry of the turbines and the aerodynamic properties of the blade sections [22]. The coupling of the ALM and OpenFOAM is based on the *turbinesFoam* implementation[38].

The computations were carried out using a DES model. The DES model is a hybrid URANS-LES approach that aims at resolving the boundary layer using the RANS approach and to simulate the detached eddies with LES [39]. The switch between the two models depends upon a local length scale d, computed as:

$$d = \min(d, C_{DES}\Delta)$$

where d is the wall distance for RANS computations, C_{DES} is usually a constant value depending on the turbulence model and set to 0.61 in this case. The value of Δ is given by the maximum cell length, is evaluated for each cell, and determined by the grid resolution. In such formulation, the term d

controls the switch between the URANS and LES. In the standard DES k-ω SST formulation, if the wall-tangential dimensions of the cells are smaller than the boundary layer thickness, the LES formulation is used in place of the URANS model, leading to incorrect predictions. This limitation is overcome by the DDES model, that corrects the length scale *d* by introducing a blending function that depends on the velocity gradients and both the kinematic and turbulent viscosities [40].

3. Definition of the case study and simulations

The target site selected for this study is the location of the FINO2 platform [41], an offshore research platform located in the Baltic Sea (55° 00' 24.94'' N, 13° 09' 15.08'' E), 35 km from the land. For this location, LIDAR wind measurements are available for a period ranging from July 2011 to July 2012 [42]. Screening the measurements, we selected a winter day (15 of December 2011), to perform the 24h reanalysis using the WRF-ARW. The 10 minutes time interval extracted for this test-case is characterised by a velocity profile featuring moderate turbulence and strong wind veer in the firsts 400 meters above the sea level (a. s. l.), and it corresponds to the time frame ranging from 10:30 to 10:40.

3.1. Simulation setup and computational domain

The mesoscale grid is made up of two domains nested in two-way mode. The low-resolution domain (400 × 300 cells) covers an area of 1500 squared Mm with a grid spacing of 3.6 km; the nested grid (d02 in Fig. 1, 463 × 385 cells) covers an area of 260 squared Mm around the target location and it has a resolution of 1.2 km. WRF-ARW uses as initial and boundary conditions the analysis at 0.125 degrees of the High Resolution (HRES) model released by the European Centre for Medium-range Weather Forecasts (ECMWF). The WRF-ARW vertical grid has 40 vertical levels, ranging from the surface to an upper boundary set to 100 hPa. The vertical levels are unequally spaced featuring a first level at approximately 10 m a. s. l. and 15 levels within the PBL. The time integration scheme is a third order Runge–Kutta, with a time step of 20 s for the largest domain and to 6.67 s for the finest domain.

The day of the analysis is characterized by the presence of two dominant synoptic structures: Siberian High-pressure in the west side of Europe, and a low-pressure zone (960 hPa) centered in the north Atlantic Ocean. This baric configuration causes a strong flow from the South over the target area.

The local-scale domain has a lateral size of 4.8 km, and a vertical size set to 600 m. This size is large enough to cover the portion of the PBL occupied by the wind farm, and it is high enough to ensure that the wind velocity profile of local and meso-scale simulations match above the surface layer.

The computational mesh used for the local-scale simulations has been created using the *cfMesh* library [43]. Several levels of refinement are adopted to reduce the number of cells in the far field. Figure 2 shows a sketch of the computational domain and the refinements. In particular, the mesh has been set up to contain a refinement for the sea wave's region, an inflation layer for all the sea surface, a refinement for the wake of the two turbines, and two refinement regions for the rotors WT1 and WT2. The refinements of the rotors are different only in their extension, the one for WT1 is larger than the one of WT2, to host also a yawed rotor configuration without changing the mesh. The final mesh is a Cartesian type mesh with 22 million cells: its smallest element is 0.5 m length and 0.1 m height and the largest one 150 m wide.

The wavelength adopted for the sea waves is 30 meters, and a minimum size of 0.5 meters is imposed to the ground cells to correctly resolve the wave geometry.

Figure 3 shows the velocity boundary conditions interpolated on the local scale domain from the mesoscale solution at the initial time of the URANS simulation.

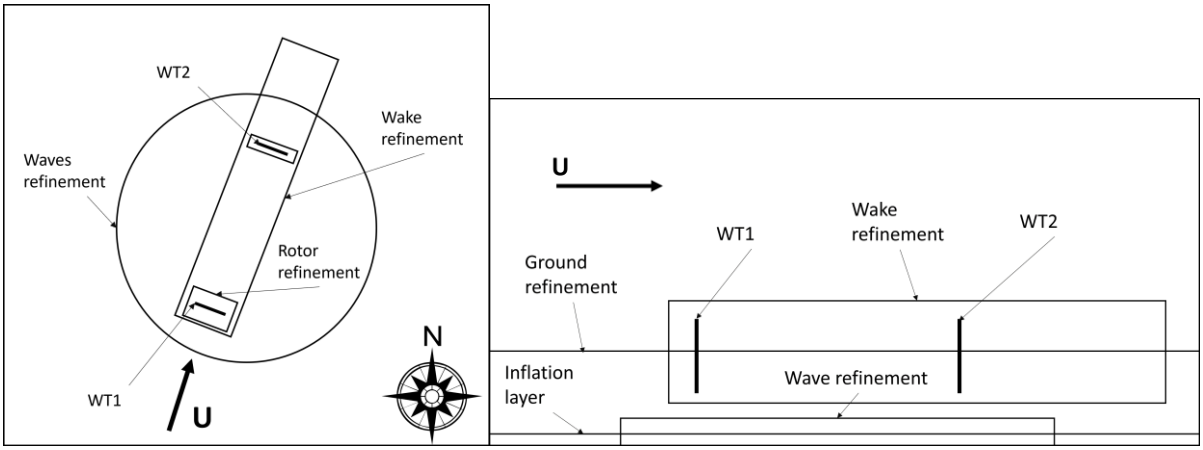

Figure 2 - Local scale computational domain, WTs location, and mesh refinement regions

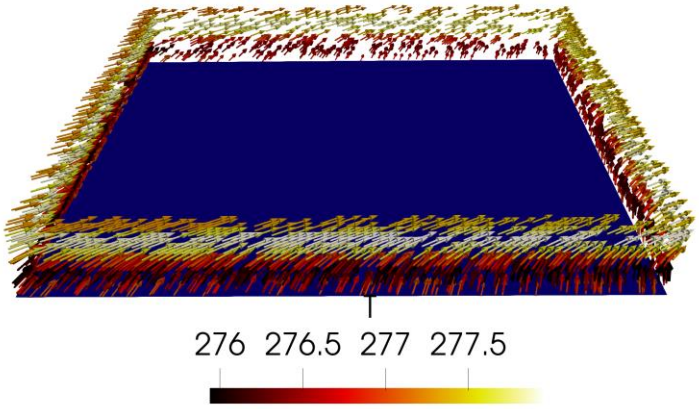

Figure 3 - Initial wind velocity and temperature at the lateral boundary patches of the local scale domain

A first steady RANS simulation is performed to initialize the flow field to the condition at 10:30 a.m., then, an URANS simulation is performed for 600 seconds to obtain the averaged wind profile without the WTs. Finally, the DDES simulation is run for 250 seconds with the two WTs simulated using the ALM. In the URANS and DDES simulations, the time dependent boundary conditions are generated and applied to the boundary patches through a table-lookup approach relying on the *timeVaryingMapped-FixedValue* and *freestream* function of the OpenFOAM library.

The SIMPLE and PIMPLE algorithms are used as non-linear solvers for the steady and unsteady simulations, respectively. The Euler first order time integration scheme with a time step of 0.05 s is used for the time-accurate discretization of the unsteady simulations. Second order upwind schemes are used for the divergence and gradient terms of the velocity, and turbulence variables. The pressure is solved using a GAMG solver, while all the other variables are evaluated with smoothSolver.

3.2. Wind turbine models, layouts and configurations

The turbine selected for this study is the DTU10, a reference off-shore wind turbine designed by Bak et al. [5][6]. The DTU10 is a three-blade upwind HAWT designed to have a rated power of 10MW at a nominal wind speed of 11.4 m/s with 9.6 rpm of rotor velocity. It has a rotor diameter of 178.3 and a hub height equal to 119 m. The turbine operates between a cut-in speed of 4 m/s and a cut-out speed of 25 m/s.

In the present study, two DTU10 turbines are placed in the computational domain at a relative distance of 7 rotor diameters. The upstream turbine (WT1) is operating at two different orientations in the two simulations: in the first one, WT1 is aligned with the main direction of the wind, while in the second simulation WT1 is oriented with a yaw angle of 20° counted positive from East to North. The downwind turbine WT2 is always aligned with the main direction of the wind.

Both turbines are modelled with the ALM, and each blade is discretized with 40 elements. The turbines operate at fixed TSR= 7.237. The tip and root effects are accounted for using the Glauert model [37]. The presence of the hub is considered for both the turbines using a drag element, while the effects of the towers are neglected.

4. Results

A first steady RANS simulation has been performed to initialize the flow field for the URANS and DDES simulations. Figure 5 shows the vertical profiles of the wind velocity magnitude, wind direction (angle of the wind velocity with respect to the x-axis), and turbulent kinetic energy, computed in the steady RANS, URANS and WRF-ARW simulations performed without the wind turbines, and averaged over the 10 minutes timeframe defined in Section 3. We can see how the velocity magnitude profile does not follow a monotonic trend, starting to decrease around 150 metres a. s. l.. The direction of the wind vector also exhibits a significant rate of rotation toward the East (x-axis direction) above 150 m a. s. l.. This behaviour is an effect of the large-scale convection in the PBL, and it could be observed and reproduced in the CFD simulations thanks to the multiscale approach adopted in this study.

The velocity and turbulence profiles of Figure 4 show also the effect of resolving the wave motion of the sea surface. The presence of waves in the URANS simulation increases turbulence in the first 50 meters a. s. l., and reduces the average wind speed, when compared with the RANS solution, which cannot account for the motion of the sea surface.

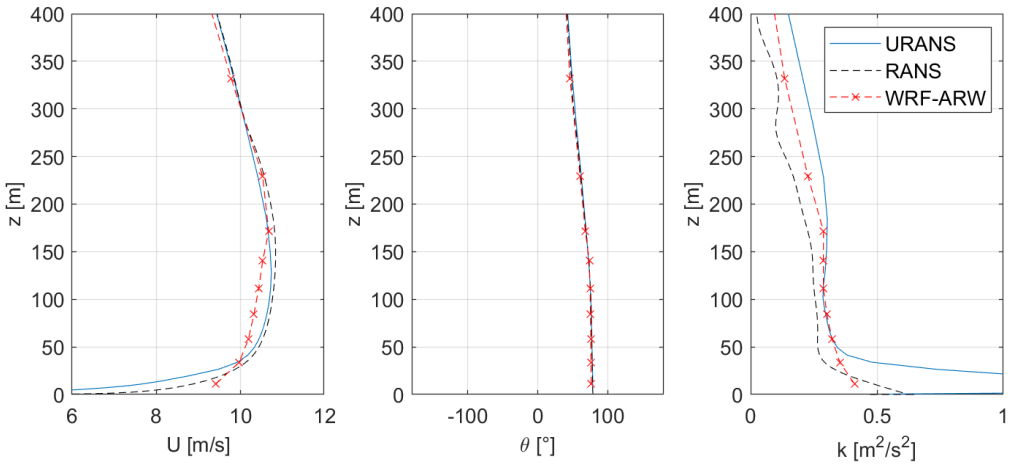

Figure 4 - Average wind vertical profile at the centre of the CFD domain, URANS simulation without the WTs

The turbine power computed in the DDES simulations with ALM is reported in Figure 5. The values are obtained by time-averaging the rotor power over a single revolution after 200 seconds of simulation. Even though the wind velocity at the hub is close to the rated value, the power output of the upstream turbine in the first simulation (no yaw) is only 7.72MW, rather than the 10MW of expected rated power. The downstream rotor only generates 4.11 MW because of the inflow velocity deficit associated with the wake of the upstream turbine. In the second (yawed) simulation, there is an additional power loss in the first wind turbine due to the yaw control, which decreases the power output from 7.72 MW to 6.84 MW. The power lost because of the yawed rotor is partially recovered by a small increase in the power generated by the downstream turbine (4.30 MW). Globally, the

yawed configuration is producing 5.8% of power less than when both rotors are aligned with the main wind.

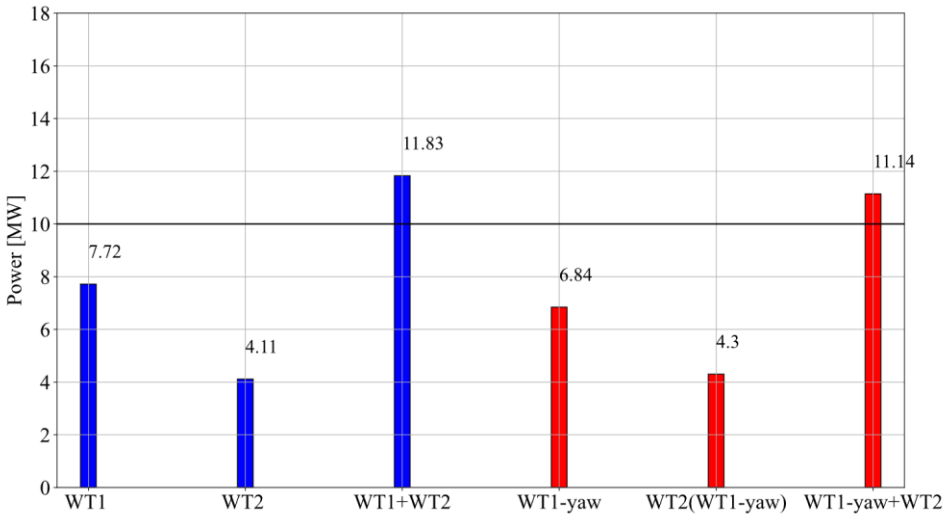

Figure 5 - Single and combined turbine power output in the two simulations

The influence of the upstream rotor misalignment can be partially analyzed by observing the velocity field.

Figure 6 shows a horizontal slice of the domain, taken at the hub height. In the first simulation, shown on the left frame of Fig. 6, the wake of the first rotor dominates the flow upstream of WT2, which operates with an inflow wind speed that is sensibly lower (4 m/s in the lowest speed portion of the wake) than the rated wind speed. In the second simulation with WT1 in yawed configuration, shown in the right frame of Fig. 6, the wake of WT1 is sensibly different. The central region of the wake, corresponding to the wake shed by the hub, interacts with the core of the wake after approximately 2 diameters. At the WT2, two major effects can be observed. First, we notice that a reduced portion of the WT2 rotor area interacts with the wake shed by WT1 with respect to the case when both rotors are aligned with the wind. A second observation has to do with the wake of WT2, which exhibits high mixing and turbulence. This effect is less pronounced in the wake computed in the first simulation. Then, the WT2 wake aligns with the main flow around 15 diameters downstream from WT2.

Figure 7 shows the section of the WTs wakes computed in the two simulations, at different axial coordinates. The slice planes are normal to the average wind direction computed at the hub height. The wake distortion in the yawed WT1 case is more pronounced in the second simulation, while in the aligned configuration, the wake is more axially symmetric. We can observe that the non-uniform wind profile affects the wake by generating a rolling effect on the wake that pushes it down, and this effect is more pronounced in the second simulation. At the rotor of WT2, a significant difference is found in terms of the shape and location of the upstream WT wake, that appears more stretched in the second simulation. Because of this deformation, the upper half of the WT2 rotor disk sees higher velocities, ranging between 8 to 11 m/s, with respect to the aligned setup. This observation can be also seen in Figure 8, which shows a slice of the velocity field in a plane defined by the main wind direction and the vertical axis. Figure 8 also shows a stronger interaction between the boundary layer developed over the sea waves and the aligned WT1 wake, as observable from the presence of a high-speed region in the area above the sea surface, immediately upstream of WT2.

A visualization of the turbulent structures can be performed by using the Q criterion. Figure 9 shows iso-surfaces of Q = 0.001 coloured using the flow velocity magnitude. It is possible to see how the wind-rotor misalignment of WT1 induces a deformation of the tip vortices and a deflection of the

wake's core trajectory. The higher turbulence produced by the interaction between the yawed WT wake and the second rotor is also highlighted in this figure.

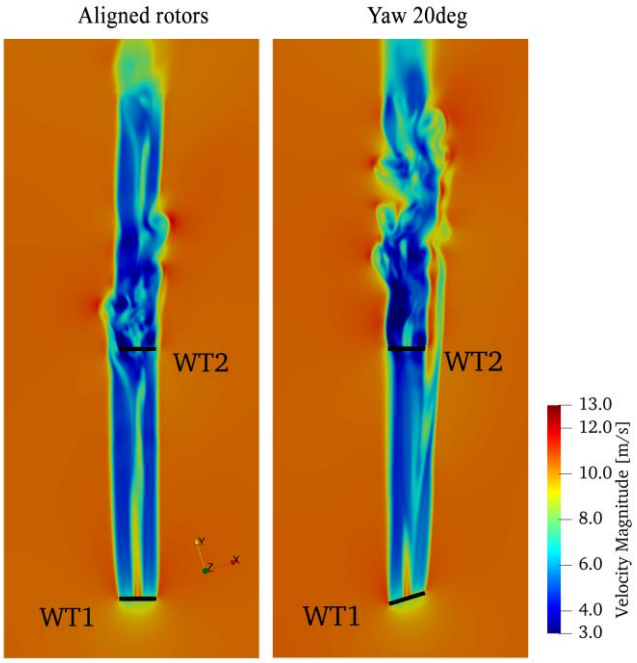

Figure 6 - Comparison between the aligned and yawed cases: instantaneous velocity fields at h = 119 m (hub height)

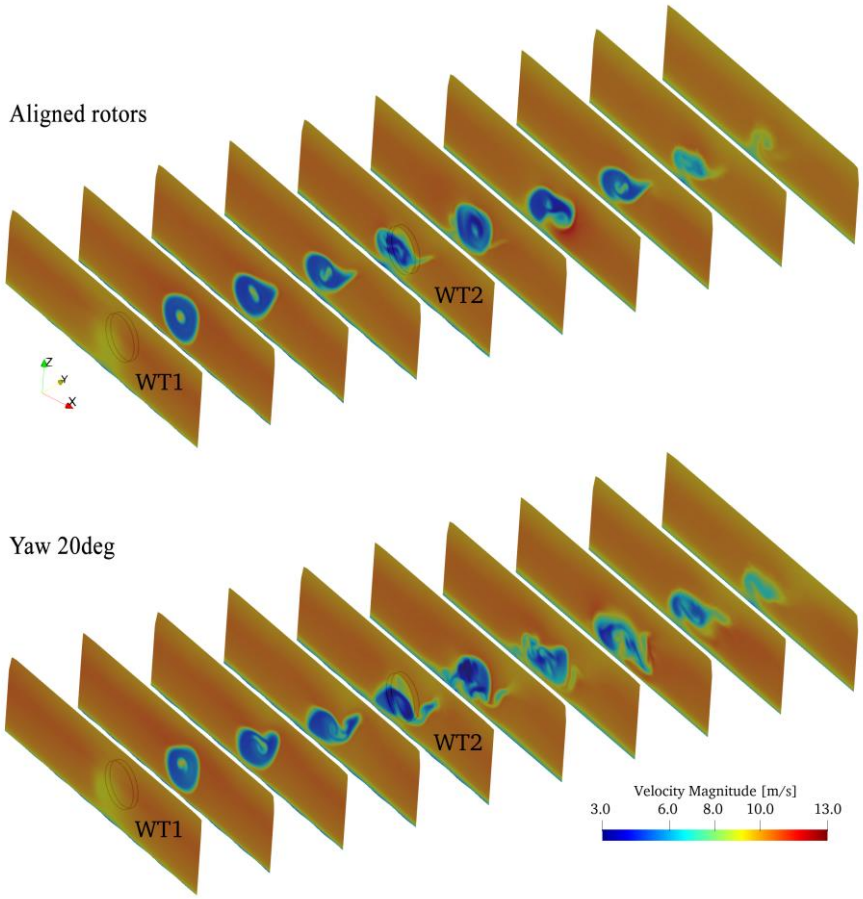

Figure 7 - Comparison between the aligned and yawed cases: spatial development of the wakes at different axial coordinates

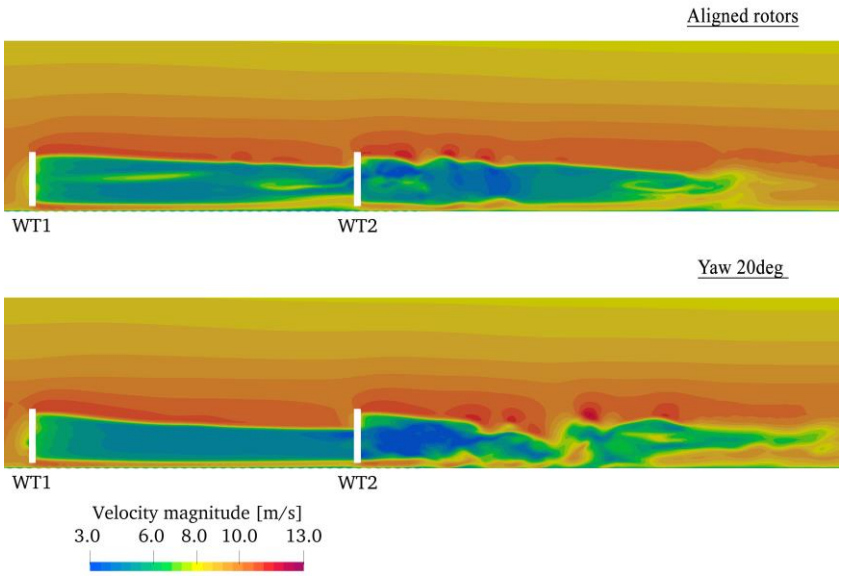

Figure 8 - Comparison of the two cases: instantaneous velocity on a vertical plane

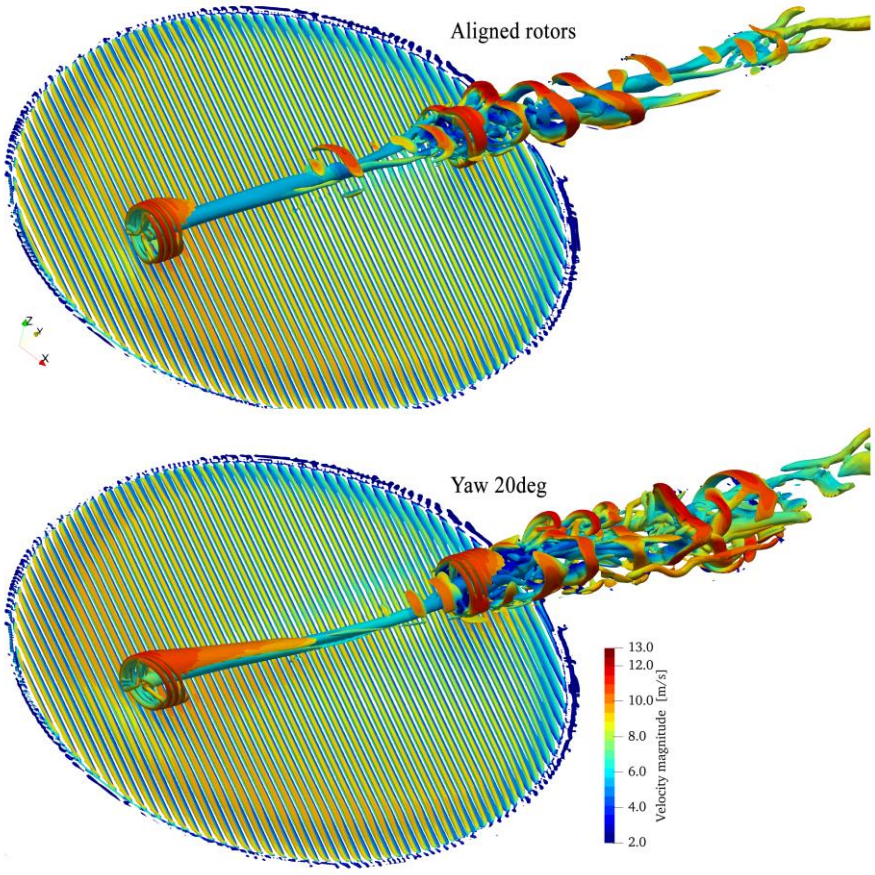

Figure 9 - Comparison between the aligned and yawed configurations: iso-surfaces of Q=0.001 coloured with instantaneous velocity

5. Conclusions

The paper reports the results of numerical simulations performed to study the aerodynamics of an offshore wind farm composed of two 10 MW wind turbines. The objective is to verify, using high fidelity numerical analyses, the interactions between a realistic wind field, the wind turbines wakes, and the rotors. Two sample setups have been investigated in the framework of wake loss analysis and control. In both cases the two rotors are aligned with the main wind direction; in the first configuration the two rotor axes are aligned with the main wind direction, while in the second configuration, a nonzero yaw angle is prescribed to the upstream rotor.

The wind field simulation is based on a multi-scale approach, in which boundary conditions for the local-scale CFD simulations are generated using a meso-scale NWP tool. The downscaling procedure allows the mesoscale solution to be interfaced with a local-scale CFD simulation based on either RANS or DDES models, thus obtaining a higher spatial resolution of the wind field than it is possible using NWP alone. The presence of the wind turbines is then simulated using the ALM, achieving a high accuracy of the aerodynamic field of the wakes at a sustainable computational cost.

In the testcase examined, we observed that yawing the first rotor does not seem to improve the overall performance of the wind farm. Indeed, the yaw angle of the WT1 induces a deviation of the wake that interacts with a smaller portion of the WT2 rotor. Therefore WT2 produces more power than in the case with both rotors aligned. However, this effect is not sufficient to recover the power lost by having the WT1 working in misaligned condition. The interaction of the wake with the second rotor gives rise to higher turbulence in the yawed condition than when both rotors are aligned. The results show also significant interference of the wind veer on the wake generation and transport.

6. References

[1] Gebraad, P. M., Teeuwisse, F. W., Van Wingerden, J. W., Fleming, P. A., Ruben, S. D., Marden, J. R., & Pao, L. Y. (2016). Wind plant power optimization through yaw control using a parametric model for wake effects—a CFD simulation study. Wind Energy, 19(1), 95-114.
[2] Campagnolo, F., Petrović, V., Schreiber, J., Nanos, E. M., Croce, A., & Bottasso, C. L. (2016, September). Wind tunnel testing of a closed-loop wake deflection controller for wind farm power maximization. In Journal of Physics: Conference Series (Vol. 753, No. 3, p. 032006). IOP Publishing.
[3] Porté-Agel, F., Wu, Y. T., Lu, H., & Conzemius, R. J. (2011). Large-eddy simulation of atmospheric boundary layer flow through wind turbines and wind farms. Journal of Wind Engineering and Industrial Aerodynamics, 99(4), 154-168.
[4] E. Gaertner, J. Rinker, L. Sethuraman, F. Zahle, B. Anderson, G. Barter, N. Abbas, F. Meng, P. Bortolotti, W. Skrzypinski, et al., "Definition of the iea wind 15-megawatt offshore reference wind turbine", Technical report, National Renewable Energy Laboratory, Golden, Mar, 2020.
[5] Bak, Christian, Frederik Zahle, Robert Bitsche, Taeseong Kim Anders Yde, Lars Christian Henriksen, Anand Natarajan, and Morten Hartvig Hansen. 2013. *Description of the DTU 10 MW Reference Wind Turbine*. Roskilde, DK: DTU Wind Energy. DTU Wind Energy Report-I-0092.
[6] Bak, Christian, Frederik Zahle, Robert Bitsche, Taeseong Kim Anders Yde, Lars Christian Henriksen, Morten Hartvig Hansen, José Pedro Albergaria Amaral Blasques, Mac Gaunaa, and Anand Natarajan. 2013 (May 27 - May 28). *The DTU 10-MW Reference Wind Turbine* (Conference Presentation). Danish Wind Power Research 2013, Fredericia, Denmark. https://orbit.dtu.dk/en/publications/the-dtu-10-mw-reference-wind-turbine.
[7] A. Castorrini, S. Gentile, E. Geraldi, and A. Bonfiglioli, "Increasing spatial resolution of wind resource prediction using nwp and rans simulation", Journal of Wind Engineering and Industrial Aerodynamics, 210 (2021) 104499
[8] M. Tewari, H. Kusaka, F. Chen, W.J. Coirier, S. Kim, A.A. Wyszogrodzki, and T.T. Warner, "Impact of coupling a microscale computational fluid dynamics model with a mesoscale model on urban scale contaminant transport and dispersion", Atmospheric Research, 96 (2010) 656–664.
[9] B. Blocken, W. Janssen, and T. van Hooff, "Cfd simulation for pedestrian wind comfort and wind safety in urban areas: General decision framework and case study for the eindhoven university campus", Environmental Modelling & Software, 30 (2012) 15–34
[10] V.J. Duraisamy, E. Dupont, and B. Carissimo, "Downscaling wind energy resource from mesoscale to microscale model and data assimilating field measurements", Journal of Physics: Conference Series, 555 (2014) 012031, doi: 10.1088/1742-6596/555/1/012031.
[11] P. Duràn, C. Meiβner, and P. Casso, "A new meso-microscale coupled modelling framework for wind resource assessment: A validation study", Renewable Energy, 160 (2020) 538–554.
[12] D. Leukauf, A. El-Bahlouli, K. zum Berge, M. Sch¨on, H. Knaus, and J. Bange, "The impact of a forest parametrization on coupled wrf-cfd simulations during the passage of a cold front over the winsent test-site", Wind Energy Science Discussions, 2019 (2019) 1–24.
[13] Y. Liu, S. Miao, C. Zhang, G. Cui, and Z. Zhang, "Study on micro-atmospheric environment by coupling large eddy simulation with mesoscale model", Journal of Wind Engineering and Industrial Aerodynamics, 107-108 (2012) 106–117, doi: https://doi.org/10.1016/j.jweia.2012.03.033
[14] P. Richards and R. Hoxey, "Appropriate boundary conditions for computational wind engineering models using the k-epsilon turbulence model", Journal of wind engineering and industrial aerodynamics, 46 (1993) 145–153.
[15] O. Temel, S. Porchetta, L. Bricteux, and J. van Beeck, "Rans closures for non-neutral microscale cfd simulations sustained with inflow conditions acquired from mesoscale simulations", Applied Mathematical Modelling, 53 (2018) 635–652.

[16] A. Sogachev, M. Kelly, and M.Y. Leclerc, "Consistent two-equation closure modelling for atmospheric research: buoyancy and vegetation implementations", Boundary-layer meteorology, 145 (2012) 307–327
[17] Thé, J., & Yu, H. (2017). A critical review on the simulations of wind turbine aerodynamics focusing on hybrid RANS-LES methods. *Energy*, *138*, 257-289.
[18] Strelets, M. (2001, January). Detached eddy simulation of massively separated flows. In 39th Aerospace sciences meeting and exhibit (p. 879).
[19] Schulz, C., Klein, L., Weihing, P., & Lutz, T. (2016, September). Investigations into the interaction of a wind turbine with atmospheric turbulence in complex terrain. In Journal of Physics: Conference Series (Vol. 753, No. 3, p. 032016). IOP Publishing.
[20] Johansen, J., Sørensen, N. N., Michelsen, J. A., & Schreck, S. (2002). Detached-eddy simulation of flow around the NREL Phase VI blade. Wind Energy: An International Journal for Progress and Applications in Wind Power Conversion Technology, 5(2-3), 185-197.
[21] Rahimi, H., Dose, B., Herraez, I., Peinke, J., & Stoevesandt, B. (2016). DDES and URANS comparison of the NREL phase-VI wind turbine at deep stall. In 34th AIAA applied aerodynamics conference (p. 3127).
[22] Sorensen, J. N., & Shen, W. Z. (2002). Numerical modeling of wind turbine wakes. J. Fluids Eng., 124(2), 393-399.
[23] Troldborg, N., Sorensen, J. N., & Mikkelsen, R. (2010). Numerical simulations of wake characteristics of a wind turbine in uniform inflow. Wind Energy: An International Journal for Progress and Applications in Wind Power Conversion Technology, 13(1), 86-99.
[24] Troldborg, N., Sørensen, J. N., & Mikkelsen, R. (2007, July). Actuator line simulation of wake of wind turbine operating in turbulent inflow. In Journal of physics: conference series (Vol. 75, No. 1, p. 012063). IOP Publishing.
[25] Churchfield, M., Lee, S., Moriarty, P., Martinez, L., Leonardi, S., Vijayakumar, G., & Brasseur, J. (2012, January). A large-eddy simulation of wind-plant aerodynamics. In 50th AIAA aerospace sciences meeting including the new horizons forum and aerospace exposition (p. 537).
[26] Stevens, R. J., Martínez-Tossas, L. A., & Meneveau, C. (2018). Comparison of wind farm large eddy simulations using actuator disk and actuator line models with wind tunnel experiments. Renewable energy, 116, 470-478.
[27] Sørensen, J. N., Mikkelsen, R. F., Henningson, D. S., Ivanell, S., Sarmast, S., & Andersen, S. J. (2015). Simulation of wind turbine wakes using the actuator line technique. Philosophical Transactions of the Royal Society A: Mathematical, Physical and Engineering Sciences, 373(2035), 20140071.
[28] W.C. Skamarock, J.B. Klemp, J. Dudhia, D.O. Gill, Z. Liu, J. Berner, W. Wang, J.G. Powers, M.G. Duda, D.M. Barker, et al., "A description of the advanced research wrf model version 4.3", Technical Report NCAR/TN-556+STR, Natl. Ctr. Atmos. Res., Boulder, CO, 2021, doi:10.5065/1dfh-6p97.
[29] W.Wang, C. Bruy`ere, M. Duda, J. Dudhia, D. Gill, M. Kavulich, K. Keene, M. Chen, H. Lin, J. Michalakes, et al.,"Wrf-arw version 3 modeling system user's guide", Technical report, National Centre for Atmospheric Research, 2009.
[30] M. Nakanishi and H. Niino, "An improved mellor–yamada level-3 model with condensation physics: Its design and verification", Boundary-layer meteorology, 112 (2004) 1–31
[31] D. Hargreaves and N.G. Wright, "On the use of the k–ε model in commercial cfd software to model the neutral atmospheric boundary layer", Journal of wind engineering and industrial aerodynamics, 95 (2007) 355–369.
[32] H. Charnock, "Wind stress on a water surface", Quarterly Journal of the Royal Meteorological Society, 81 (1955) 639–640.
[33] Y. Goda, Random seas and design of maritime structures, volume 33. World Scientific Publishing Company,2010.

[34] H. Jasak, "Dynamic mesh handling in openfoam", in 47th AIAA aerospace sciences meeting including the new horizons forum and aerospace exposition, (2009) 341.
[35] J. Davidson, M. Karimov, A. Szelechman, C. Windt, and J. Ringwood, "Dynamic mesh motion in openfoam for wave energy converter simulation", in 14th OpenFOAM Workshop, (2019).
[36] H.G. Weller, G. Tabor, H. Jasak, and C. Fureby, "A tensorial approach to computational continuum mechanics using object-oriented techniques", Computers in physics, 12 (1998) 620–631.
[37] Glauert, H. (1935). Airplane propellers. In Aerodynamic theory (pp. 169-360). Springer, Berlin, Heidelberg.
[38] Bachant, P., Goude, A., & Wosnik, M. (2016). Actuator line modeling of vertical-axis turbines. *arXiv preprint arXiv:1605.01449*.
[39] Davidson, L. (2015). Fluid mechanics, turbulent flow and turbulence modeling.
[40] Spalart, P. R., Deck, S., Shur, M. L., Squires, K. D., Strelets, M. K., & Travin, A. (2006). A new version of detached-eddy simulation, resistant to ambiguous grid densities. Theoretical and computational fluid dynamics, 20(3), 181-195.
[41] F.R.P. in the Baltic Sea. Available online: https://www.fino2.de/en
[42] Ørsted Open Data Service. Available online: https://orsted.com/en/our-business/offshore-wind/wind-data, Accessed on 12 March 2021
[43] F. Juretic, "cfmesh user guide", Creative Fields, Ltd, 1 (2015).

Acknowledgments
The authors acknowledge funding support from the Italian Ministry of Education, University and Research through the Programma Operativo Nazionale Ricerca e Innovazione 2014-2020 (CUP - 34I19000050006, Activity – AIM 1859451/3). The work has been also partially performed under Project HPC-EUROPA3 (INFRAIA-2016-1-730897), with the support of the EC Research Innovation Action under the H2020 Programme; in particular, the authors gratefully acknowledge the support of M.S. Campobasso from the Engineering Department at Lancaster University, and the computer resources and technical support provided by EPCC at The University of Edinburgh.